Human adherent cortical organoids in a multiwell format

Mark van der Kroeg[1], Sakshi Bansal[1], Maurits Unkel[1], Hilde Smeenk[1,] Steven A. Kushner[1,2,3#*], Femke M.S. de Vrij[1,4#*]

[1]Department of Psychiatry, Erasmus MC, Rotterdam, 3015 CN, The Netherlands.

[2]Dept. of Psychiatry, Columbia University Irving Medical Center, New York, NY, USA

[3]Stavros Niarchos Foundation (SNF) Center for Precision Psychiatry & Mental Health, Columbia University, New York, NY, USA

[4]ENCORE Expertise Center for Neurodevelopmental Disorders, Erasmus MC, Rotterdam, NL

[#]These authors contributed equally

Contact information: *Correspondence: sk2602@cumc.columbia.edu, f.devrij@erasmusmc.nl.

Summary

In the growing diversity of human iPSC-derived models of brain development, we present here a novel method that exhibits 3D cortical layer formation in a highly reproducible topography of minimal dimensions. The resulting adherent cortical organoids develop by self-organization after seeding frontal cortex patterned iPSC-derived neural progenitor cells in 384-well plates during eight weeks of differentiation. The organoids have stereotypical dimensions of 3 x 3 x 0.2 mm, contain multiple neuronal subtypes, astrocytes and oligodendrocyte lineage cells, and are amenable to extended culture for at least 10 months. Longitudinal imaging revealed morphologically mature dendritic spines, axonal myelination, and robust neuronal activity. Moreover, adherent cortical organoids compare favorably to existing brain organoid models on the basis of robust reproducibility in obtaining topographically-standardized singular radial cortical structures and circumvent the internal necrosis that is common in free-floating cortical organoids. The adherent human cortical organoid platform holds considerable potential for high-throughput drug discovery applications, neurotoxicological screening, and mechanistic pathophysiological studies of brain disorders.

Introduction

Using human embryonic or induced pluripotent stem cell (hiPSC) derived models to investigate the developing brain in health and disease has yielded considerable success (Marton and Paşca, 2020). The approaches have been varied, including single cell hiPSC-derived models grown in a monolayer (Sarkar et al., 2018; Zhang et al., 2013), multiple neural cell types in 2D neural networks (Astick and Vanderhaeghen, 2018; Bardy et al., 2015; Gunhanlar et al., 2018; Shi et al., 2012), 3D free-floating regionalized neural organoids (Paşca et al., 2015; Qian et al., 2016a; Xiang et al., 2019; Zhang et al., 2023), and hiPSC-derived free-floating unguided neural organoids (Gomes et al., 2020; Lancaster et al., 2013; Paşca et al., 2022; Pellegrini et al., 2020; Renner et al., 2017; Sawada et al., 2020). Among the consistent findings across models is that increasing cellular and topographical complexity has appeared to come at the cost of increased variability (Eichmüller and Knoblich, 2022; Kelava and Lancaster, 2016). Therefore, a major current technical challenge is to identify hiPSC-derived models that recapitulate higher-order neural complexity with reduced heterogeneity.

Existing 3D models suffer from considerable variability due to the complex and heterogeneous nature of the free-floating structures (Cederquist et al., 2019; Lancaster et al., 2013, 2017; Paşca et al., 2015; Renner et al., 2017; Velasco et al., 2019; Yoon et al., 2019). A further challenge, in particular with free-floating organoids, is the necrotic core that emerges when tissue volumes exceed the limits of oxygen and nutrient diffusion beyond a radius of ~300-400μm (Lancaster et al., 2017; Qian et al., 2016b). Although recent progress has been made with slicing organoids prior to the emergence of necrosis followed by organotypic air-liquid interface culture (Giandomenico et al., 2019; Qian et al., 2020), even sliced organoids have to be repeatedly re-cut to prevent necrosis (Qian et al., 2020),

64 which is both laborious and risks introducing another potential source of variability. The
65 generation of vascularized organoids would be the ultimate solution to reduce the necrotic
66 core and the inherent stress that is observed in cortical organoids (Bhaduri et al., 2020; Fan
67 et al., 2022). It will be beneficial to have increased diffusion through microfluidics or
68 vascularization (current efforts summarized in Matsui et al., 2021) and further study the
69 mutually beneficial interaction of neural cells and vascular cells (Crouch et al., 2022;
70 Mansour et al., 2018; Wang et al., 2023).

71 Here we propose a simplified approach to generating long-term hiPSC-derived adherent
72 cortical organoids with reproducible dimensions and the potential for high-throughput
73 screening in a 384-well format. The resulting adherent cortical organoids can be maintained
74 in long-term culture and contain neurons with dendritic spines and robust activity, as well as
75 several classes of glial cells including oligodendrocyte precursor cells, myelinating
76 oligodendrocytes, and morphologically distinct sub-types of astrocytes.

77

78 **Results**

79 ***Self-organized topography of iPSC-derived adherent cortical organoids***

80 Adherent cortical organoids reproducibly self-organized into layered radial structures in
81 384-wells plates within 8 weeks of seeding with hiPSC-derived forebrain-patterned neural
82 progenitor cells (NPCs). Three different hiPSC source cell lines were used in this study,
83 including commercially available NPCs, and NPCs generated using a modified version of our
84 previously described protocol (Gunhanlar et al., 2018) (**Figure 1A**). NPCs were capable of
85 neural rosette formation and expressed SOX2, Nestin, and the frontal cortical NPC-marker
86 FOXG1 (**Figure 1B, C, D, Figure S1A).** The initial 4 weeks after seeding the NPCs in Neural
87 Differentiation Medium (ND) were characterized by proliferative expansion of NPCs and the
88 emergence of early neural differentiation markers (**Figure 1E, Figure S2**). Between 4- and 8-
89 weeks post-seeding, neurons and glial cells emerged with a consistent spatial organization
90 (**Figure 1E, F, Figure S1B, Figure S2**), in which the central region was densely packed with
91 cell bodies while the periphery contained circumferentially and radially organized processes
92 originating from cells in the centre. Typically, cortical organoids defined as a single radial
93 structure per well were observed in ~80% of the wells seeded with NPCs after 60 days of
94 differentiation. The structural integrity of single structure organoids remained quite stable
95 and slowly diminished over time to about 50% of intact single structure organoids after 1
96 year in culture (**Figure S1D**). Organoid structure formation was highly dependent on the
97 proliferation rate of NPCs, that can differ substantially between differentiation batches and
98 hiPSC clones. Plotting the interaction between proliferation and the amount of NPCs
99 required to be seeded for the successful generation of adherent cortical organoids, showed
100 a significant correlation (r^2=0.67) that can be used as a guideline for testing a range of NPC
101 densities (**Figure S1C**). For each NPC line an optimal seeding density was estimated based on

102 the proliferation rate of that NPC line. Multiple densities were seeded around the estimated
103 optimal density and after 6 weeks it was visually determined which NPC density enabled
104 adherent cortical organoid generation. Typically, too sparse seeding density generated
105 neural networks lacking structure, while excessive densities resulted in overgrowth, leading
106 to reduced structural organisation and compromised long-term survival.
107
108
109 ***Cell type distribution and layer formation***
110 The spatial organisation that evolved over the first 8 weeks after seeding was paralleled
111 by a shift in cell type distribution. Tau+/MAP2- axons exhibited long extensions in a circular
112 pattern, while MAP2+ dendrites exhibited orthogonally-oriented radial outgrowth (**Figure**
113 **2A, Figure S3**).
114 Overall, a reduction in progenitor markers (SOX2 day 14: 58.4%, day 56: 18.8% P =
115 <0.001, PAX6 day 14: 34.5%, day 56: 8.0% P = 0.20) and a significant increase in neuronal
116 cortical layer markers (CTIP2 day 14: 0.5%, day 56: 14.0% P = <0.001, CUX1 day 14: 1.3%,
117 day 56: 24.4% P = <0.001) were observed (**Figure S2**). Cortical layer markers exhibited an
118 inside-out pattern of development in which expression of the deep layer excitatory
119 neuronal marker CTIP2 emerged before the upper layer marker CUX1 (**Figure S2**, **Figure 2C**).
120 After 6-8 weeks following seeding, a self-organised rudimentary segregation of deep- and
121 upper layer neurons emerged as shown by a clear macroscopic separation of deep- and
122 upper layer neurons, although some neurons were spatially intermixed and some neurons
123 were double-positive for CTIP2 and CUX1. Segregation was also observed between CUX1
124 and CUX2 positive cells as CUX2 is typically expressed over a wider range of upper cortical
125 layers than CUX1 and also marks intermediate progenitors (Molyneaux et al., 2007) (**Figure**

126 **2C, Figure S4**). Analogous to the broad distribution of cortical cell subclasses, the majority of
127 the neurons were glutamatergic, while GAD67+ interneurons were also present (**Figure 2D**),
128 constituting ~10% of the NeuN-positive neuronal population consistently for all three
129 source hiPSC lines (**Figure S5**).
130
131 ***Adherent cortical organoids contain multiple glial cell types***
132 Within 8 weeks of seeding, a population of GFAP+/S100β+ astrocytes emerged. Many
133 astrocytes had their soma located in the central region with process outgrowth radially
134 (**Figure 2E, Figure S6**), while other astrocytes exhibited subtype-specific morphologies
135 including fibrous astrocytes (**Figure 2F**), protoplasmic-like astrocytes (**Figure 2G**) and
136 interlaminar astrocytes (**Figure 2H**). GFAP/PAX6 double-positive radial glia were present at
137 the outskirts of the densely populated centre of the organoid with processes growing
138 radially outwards (**Figure 2I**). Similar to free-floating organoids, adherent cortical organoids
139 survived for longer periods compared to monolayer neural cultures grown on larger
140 surfaces. The longevity allows for the development of cell types not usually seen in a
141 monolayer culture that can typically be cultured up to a maximum of 2 to 3 months. By 6
142 weeks after seeding NPCs we observed the emergence of oligodendrocyte precursor cells
143 (OPC), as shown by the expression of NG2 (**Figure 3A**). NG2+ cells remained present until at
144 least 4 months **(Figure 3B/C)**. Staining for Myelin Basic Protein (MBP) revealed the
145 emergence of MBP+ oligodendrocytes around 4 months after NPC seeding when the
146 organoids were continuously grown in the presence of T3 (2ng/ml) **(Figure 3D)**. At 5 months,
147 the oligodendrocytes showed increasingly mature morphologies (**Figure 3E-I**) and exhibited
148 MBP co-localization along NF200+ axons (**Figure 3F/I**).
149

150 ***Adherent cortical organoids show synaptic connectivity and functional activity***

151 Neurons within adherent cortical organoids exhibited clear evidence of synaptogenesis
152 (**Figure 4A-D**). Sparse labelling of excitatory neurons with AAV9.CamKII.eGFP revealed the
153 presence of Synapsin-positive (Syn+) mushroom-shaped dendritic spines (**Figure 4E**). To
154 assess the functional activity of the cortical organoids, we used the genetically-encoded
155 calcium indicator GCaMP6s under the control of the human Synapsin promoter (**Figure 4F**),
156 allowing cell-type specific quantification of neuronal activity. Calcium imaging revealed
157 robust synchronous network-level bursting (NB) (1.4 $\pm$ 0.07 NB/min) in which the vast
158 majority of recorded neurons participated. In addition, substantial desynchronized activity
159 was also observed (3.9 $\pm$ 0.5 events/min) during time periods outside of network-level
160 bursting (**Figure 4G-J, Figure 4 – Video 1**).

161

162 **Discussion**

163 The study of early human brain development and related diseases has long been hampered
164 by the inherent complexity of the human brain and the inaccessibility of living brain tissue at
165 cellular resolution. Technological advances in induced pluripotent stem cell technology have
166 now facilitated the opportunity to obtain living human neurons derived from specific
167 individuals.

168 We describe here a platform to model early human frontal cortical development with high
169 reproducibility and simplified organization. While 3D floating organoids, or sliced organoids,
170 nicely recapitulate layered cortex formation, they are subject to variation in the relative
171 contribution of cortical tissue within the organoid, forming multiple cortical patches along
172 the edges and complicating structured analysis (Eichmüller and Knoblich, 2022;
173 Giandomenico et al., 2019; Quadrato et al., 2017). Moreover, 3D floating organoids suffer

174 from necrosis in the core of the organoid due to lack of oxygen and nutrient diffusion.
175 Recently, other protocols have been published starting from rosette formation with a focus
176 on very early development and leading to single structure free floating cortical
177 organoids(Pagliaro et al., 2023; Tidball et al., 2023). Our platform predefines a rosette-
178 forming iPSC-derived cortical NPC population that self-organizes into adherent singular
179 radial structures in a standard 384-well format. Other examples have highlighted the
180 benefits of a multi-well format or systematic individual structure formation (Knight et al.,
181 2018; Medda et al., 2016). Our platform now integrates these features to yield individual
182 adherent layered cortical structures with robust functional synaptic connectivity and
183 neuronal activity and including advanced glial cell types such as myelinating
184 oligodendrocytes and subclasses of astrocytes. The small reproducible format of the
185 organoids in a 384-well format has the distinct advantage of being able to image entire
186 organoids without slicing or clearing and to perform spatiotemporal functional analysis by
187 fluorescence-based calcium imaging. We confirmed the self-organizing potential and
188 reproducibility of adherent cortical organoids across multiple hiPSC lines and using different
189 sources of NPCs, controlling the seeding density for the proliferation rate of the specific NPC
190 batch. Seeding NPCs with frontal cortical identity in the defined geometry of a 384-well plate
191 enabled the development of long-term functional neural networks in a complex radial
192 structure resembling early human cortical development. Future studies aimed at single cell
193 gene expression analysis and advanced image-based analysis solutions in this platform will
194 be interesting in the context of the increasing knowledge on single cell topographical,
195 typological and temporal hierarchies in the developing human cortex (Bhaduri et al., 2021;
196 Nowakowski et al., 2017, 2016; Uzquiano et al., 2022).

These functional adherent cortical organoids in a multi-well format should be amenable to high-throughput screening applications, mechanistic pathophysiological studies of neurodevelopmental and neuropsychiatric disorders, and pharmacological and phenotypic screening of disease phenotypes during early cortical development. Moreover, toxicological studies for novel therapeutic compounds also show an increasing need for testing specific effects in human neuronal models, whereas studies using rodent models have often shown poor predictive power for drug safety and efficacy in human central nervous system disorders (van Esbroeck et al., 2017).

Adherent cortical organoids also have some limitations, as the current iteration of adherent cortical organoids exhibits limited cortical layering and regional specification, that seem to be more advanced in floating whole brain organoids. However, these drawbacks are offset by significantly enhanced ease and higher-throughput possibilities of downstream analysis applications.

Taken together, we present a novel platform for cellular-level human brain modeling using adherent cortical organoids that exhibit high reproducibility and robust neuronal activity. The ability to reliably generate human cortical organoids in multi-well plates combined with neural network functionality offers a unique potential for brain disease modeling and therapeutic screening applications.

217 **Materials and Methods**

218 ***Generation of Neural Progenitor Cells***

219 NPCs from 3 different source hiPSC lines were used. NPC-line 1: in house generated NPCs
220 from human iPSC line WTC11 (Provided by Bruce R. Conklin, The Gladstone Institutes and
221 UCSF, #GM25256, RRID:CVCL_Y803, Miyaoka et al.,2014). NPC-line 2: commercially available
222 hNPCs from Axol Biosciences (ax0015). NPC-line 3: NPCs derived using the protocol of Shi et
223 al., (Shi et al., 2012) from hiPSC line IPSC0028 (Sigma-Aldrich, RRID:CVCL_EE38). Line 1 NPCs
224 were generated as previously described from hiPSCs grown on a mouse embryonic
225 fibroblast (MEF) feeder layer (Gunhanlar et al., 2018). After passage 3, NPC cultures were
226 purified using fluorescence-activated cell sorting (FACS). NPCs were detached from the
227 culture plate using Accutase (Stem Cell Technologies) and $CD184^{+}/CD44^{-}/CD271^{-}/CD24^{+}$ cells
228 (Yuan et al., 2011) were collected on a FACSAria III Cell Sorter (BD Bioscience) and expanded
229 in NPC medium consisting of: DMEM/F12, 1% N2 supplement, 2% B27-RA supplement
230 (Thermo Fisher Scientific), 1 µg/ml laminin (L2020, Sigma-Aldrich), 20 ng/ml basic fibroblast
231 growth factor (Merck-Millipore, Darmstadt, Germany) and 1% penicillin/streptomycin
232 (Thermo Fisher Scientific). NPCs were differentiated to adherent cortical organoids between
233 passage 3 and 7 after sorting.

234

235 ***Neural differentiation***

236 384-well plates (M1937-32EA. Life Technologies) were coated with 50 µg/ml laminin in dH_20
237 (Sigma, L2020) for 30 minutes at 37 °C. The NPCs in NPC medium were dissociated with
238 Accutase (Stem Cell Technologies), live cells were counted with Trypan Blue (Stem Cell
239 Technologies) in a Burker counting chamber. The NPCs were seeded in the wells of a 384-
240 well plate at defined densities for each cell line. Specifically, the optimal seeding density was

241 determined by visual inspection of the organoids between 28 to 42 days after seeding a
242 range of cell densities in the 384-well plate wells. NPCs were seeded and differentiated in
243 Neural Differentiation Medium: Neurobasal medium (Thermo Fisher Scientific), 1% N2
244 supplement (Thermo Fisher Scientific), 2% B27-RA supplement (Thermo Fisher Scientific),
245 1% minimum essential medium/non-essential amino acid (Stem Cell Technologies),
246 20 ng/ml brain-derived neurotrophic factor (ProSpec Bio), 20 ng/ml glial cell-derived
247 neurotrophic factor (ProSpec Bio), 1 µM dibutyryl cyclic adenosine monophosphate (Sigma-
248 Aldrich), 200 µM ascorbic acid (Sigma-Aldrich), 2 µg/ml laminin (Sigma-Aldrich) and 1%
249 penicillin/streptomycin (Thermo Fisher Scientific). For oligodendrocyte maturation the cells
250 were grown in the presence of 2 ng/ml T3 (Sigma-Aldrich). Cells were refreshed every 2-3
251 days.
252
253 ***Immunocytochemistry***
254 For live-dead staining, living cultures were incubated with LIVE/DEAD™ Viability/Cytotoxicity
255 Kit according to manufacturer's instructions (Thermo Fisher Scientific). For
256 immunocytochemistry adherent cortical organoids were fixed for 20-30 minutes using 4%
257 formaldehyde in phosphate-buffered saline (PBS), washed with PBS and blocked for 1 hour
258 by pre-incubation in staining buffer containing 0.05 M Tris, 0.9% NaCl, 0.25% gelatin and
259 0.5% Triton-X-100 (pH 7.4). Primary antibodies were incubated for 48-72h at 4 °C in staining
260 buffer, washed with PBS and incubated with the secondary antibodies in staining buffer for
261 2h at room temperature. The cultures were embedded in Mowiol 4-88 (Sigma-Aldrich), after
262 which confocal imaging was performed with a Zeiss LSM700 and Zeiss LSM800 confocal
263 microscope using ZEN software (Zeiss, Oberkochen, Germany). The following primary
264 antibodies were used: SOX2 (Merck-Millipore AB5603, 1:200); Nestin (Merck-Millipore

265 MAB5326, 1:200); MAP2 (Synaptic Systems 188004, 1:100); NeuN (Merck ABN78, 1:200);
266 GFAP (Merck-Millipore AB5804, 1:300); FOXG1 (Abcam AB18259, 1:200); CUX1 (Abcam
267 AB54583, 1:200); CTIP2 (Abcam AB18465, 1:100); Synapsin 1/2 (Synaptic Systems 106003,
268 1:200); and PSD95 (Thermo Fisher Scientific MA1-046, 1:100); Tau (Cell Signaling Technology
269 4019, 1:200); S100ß (Sigma-Aldrich S2532, 1:200); Pax6 (Santa Cruz sc-81649, 1:100); NG2
270 (Gift from W. Stallcup Lab, 1:100); NF200 (Sigma-Aldrich 083M4833 1:200); MBP (Abcam
271 AB7349, 1:100); GFP (Abcam ab13970, 1:100); GAD67 (Merck-Millipore MAB5406, 1:100)
272 DAPI (Thermo Fisher Scientific D1306). The following secondary antibodies were used 1:200:
273 Alexa-488, Alexa-555, Alexa-647 (Jackson ImmunoResearch, West Grove, PA, USA).
274
275 ***Sparse labelling of excitatory neurons***
276 pENN.AAV9.CamKII.4.eGFP.WPRE.rBG (Addgene viral prep # 105541-AAV9) was added to
277 the cortical organoids at day 278 ($1.68x10^8$ GC/well). The transduced cortical organoids
278 were fixed and stained at day 310.
279
280 ***Calcium imaging***
281 For calcium imaging the genetically encoded calcium indicator
282 AAV1.Syn.GCaMP6s.WPRE.SV40 (Penn Vector Core, 100843-AAV1) was added to the
283 organoids at day 42 of differentiation ($1.5x10^8$ GC/well). Recordings were performed at day
284 60 on a Zeiss LSM800 confocal microscope using ZEN software (Zeiss, Oberkochen,
285 Germany). The recordings were made with a 20x/0.8NA Ph2 Plan-Apochromat objective,
286 with a field of view of 150 × 100 µm and a pixel size of 0,3 µm. The acquisition rates of the
287 recordings were between 4-5 f.p.s. 24 hours before the recordings, the medium was
288 switched to BrainPhys Neural Differentiation Medium. BrainPhys Neuronal Media (Stem Cell

289 Technologies), 1% N2 supplement (Thermo Fisher Scientific), 2% B27-RA supplement
290 (Thermo Fisher Scientific), 1% minimum essential medium/non-essential amino acid (Stem
291 Cell Technologies), 1% penicillin/streptomycin (Thermo Fisher Scientific), 20 ng/ml brain-
292 derived neurotrophic factor (ProSpec Bio), 20 ng/ml glial cell-derived neurotrophic factor
293 (ProSpec Bio), 1 µM dibutyryl cyclic adenosine monophosphate (Sigma-Aldrich),
294 200 µM ascorbic acid (Sigma-Aldrich) and 2 µg/ml laminin (Sigma-Aldrich). The calcium
295 imaging recordings were processed using CNMF-E (Pnevmatikakis et al., 2016). Calcium
296 traces were then analysed using a custom script for event and network burst detection
297 using an algorithm written in Python (v3.8.2) (code accessibility can be requested via
298 Github).
299
300 ***Cyquant Proliferation Assay***
301 CyQUANT™ Direct Cell Proliferation Assay, C35011 (Thermo Fisher Scientific) was used
302 according to manufacturer specifications. For each time point and each of the 3 NPC lines
303 10-12 wells of a 96-well plate were seeded with NPCs (2500 NPCs per well). In addition, NPC
304 lines generated from 2 different clones from IPS line MH0159020 (Rutgers University Cell
305 and DNA Repository) were added to increase the dynamic range of the proliferation curve.
306 At 24h and 96h NPCs were frozen at -80℃. All NPC lines and timepoints were thawed, lysed
307 and measured together. Doubling time was calculated between 24h and 96h. None of the
308 wells was confluent at 96h.
309
310 ***Statistical analysis***

311 All data represent mean ± SEM. When comparing developmental markers in Figure S2 we
312 used one-way ANOVA followed by Tukey- Kramer's multiple correction test. n=3-6 images
313 taken over two wells, for each time point.
314

315 **Acknowledgements**

316 This work was supported by the Netherlands Organ-on-Chip Initiative, an NWO Gravitation
317 project funded by the Ministry of Education, Culture and Science of the government of the
318 Netherlands (024.003.001) to SAK, Hersenstichting Fellowship (F2012(1)-39) to FMSdV, an
319 Erasmus MC Human Disease Model Award to FMSdV and a Dutch ZonMw MKMD
320 Create2Solve grant (114025201) to SAK and FMSdV.
321

322 **Author contributions**

323 MvdK, SB and HS performed experiments, MU developed calcium imaging analysis
324 algorithms, FdV and SAK supervised the work, MvdK, FdV and SAK wrote the paper.
325

326 **Declaration of interests**

327 The authors declare no competing interests.
328

329 **References**

330 Astick M, Vanderhaeghen P. 2018. From Human Pluripotent Stem Cells to Cortical Circuits.
331 *Curr Top Dev Biol* **129**:67–98. doi:10.1016/bs.ctdb.2018.02.011
332 Bardy C, van den Hurk M, Eames T, Marchand C, Hernandez R V, Kellogg M, Gorris M, Galet
333 B, Palomares V, Brown J, Bang AG, Mertens J, Böhnke L, Boyer L, Simon S, Gage FH.
334 2015. Neuronal medium that supports basic synaptic functions and activity of human

335 neurons in vitro. *Proc Natl Acad Sci U S A* **112**. doi:10.1073/pnas.1504393112

336 Bhaduri A, Andrews MG, Mancia Leon W, Jung DD, Shin D, Allen D, Jung DD, Schmunk G,
337 Haeussler M, Salma J, Pollen AA, Nowakowski TJ, Kriegstein AR. 2020. Cell stress in
338 cortical organoids impairs molecular subtype specification. *Nature* 1–7.
339 doi:10.1038/s41586-020-1962-0

340 Bhaduri A, Sandoval-Espinosa C, Otero-Garcia M, Oh I, Yin R, Eze UC, Nowakowski TJ,
341 Kriegstein AR. 2021. An atlas of cortical arealization identifies dynamic molecular
342 signatures. *Nature* **598**:200–204. doi:10.1038/s41586-021-03910-8

343 Cederquist GY, Asciolla JJ, Tchieu J, Walsh RM, Cornacchia D, Resh MD, Studer L. 2019.
344 Specification of positional identity in forebrain organoids. *Nat Biotechnol* **37**:436–444.
345 doi:10.1038/s41587-019-0085-3

346 Crouch EE, Bhaduri A, Andrews MG, Cebrian-Silla A, Diafos LN, Birrueta JO, Wedderburn-
347 Pugh K, Valenzuela EJ, Bennett NK, Eze UC, Sandoval-Espinosa C, Chen J, Mora C, Ross
348 JM, Howard CE, Gonzalez-Granero S, Lozano JF, Vento M, Haeussler M, Paredes MF,
349 Nakamura K, Garcia-Verdugo JM, Alvarez-Buylla A, Kriegstein AR, Huang EJ. 2022.
350 Ensembles of endothelial and mural cells promote angiogenesis in prenatal human
351 brain. *Cell* **185**:3753-3769.e18. doi:10.1016/j.cell.2022.09.004

352 Eichmüller OL, Knoblich JA. 2022. Human cerebral organoids — a new tool for clinical
353 neurology research. *Nat Rev Neurol* **18**:661–680. doi:10.1038/s41582-022-00723-9

354 Fan W, Christian KM, Song H, Ming G li. 2022. Applications of Brain Organoids for Infectious
355 Diseases. *J Mol Biol* **434**:167243. doi:10.1016/j.jmb.2021.167243

356 Giandomenico SL, Mierau SB, Gibbons GM, Wenger LMD, Masullo L, Sit T, Sutcliffe M,
357 Boulanger J, Tripodi M, Derivery E, Paulsen O, Lakatos A, Lancaster MA. 2019. Cerebral
358 organoids at the air–liquid interface generate diverse nerve tracts with functional

359 output. *Nat Neurosci* **22**:669–679. doi:10.1038/s41593-019-0350-2

360 Gomes AR, Fernandes TG, Vaz SH, Silva TP, Bekman EP, Xapelli S, Duarte S, Ghazvini M,
361 Gribnau J, Muotri AR, Trujillo CA, Sebastião AM, Cabral JMS, Diogo MM. 2020.
362 Modeling Rett Syndrome With Human Patient-Specific Forebrain Organoids. *Front Cell*
363 *Dev Biol* **8**:1–18. doi:10.3389/fcell.2020.610427

364 Gunhanlar N, Shpak G, van der Kroeg M, Gouty-Colomer LA, Munshi ST, Lendemeijer B,
365 Ghazvini M, Dupont C, Hoogendijk WJG, Gribnau J, de Vrij FMS, Kushner SA. 2018. A
366 simplified protocol for differentiation of electrophysiologically mature neuronal
367 networks from human induced pluripotent stem cells. *Mol Psychiatry* **23**:1336–1344.
368 doi:10.1038/mp.2017.56

369 Kelava I, Lancaster MAA. 2016. Stem Cell Models of Human Brain Development. *Cell Stem*
370 *Cell* **18**:736–748. doi:10.1016/j.stem.2016.05.022

371 Knight GT, Lundin BF, Iyer N, Ashton LMT, Sethares WA, Willett RM, Ashton RS. 2018.
372 Engineering induction of singular neural rosette emergence within hPSC-derived
373 tissues. *Elife* **7**. doi:10.7554/eLife.37549

374 Lancaster M a, Renner M, Martin C-A, Wenzel D, Bicknell LS, Hurles ME, Homfray T,
375 Penninger JM, Jackson AP, Knoblich JA. 2013. Cerebral organoids model human brain
376 development and microcephaly. *Nature* **501**:373–379. doi:10.1038/nature12517

377 Lancaster MA, Corsini NS, Wolfinger S, Gustafson EH, Phillips AW, Burkard TR, Otani T,
378 Livesey FJ, Knoblich JA. 2017. Guided self-organization and cortical plate formation in
379 human brain organoids. *Nat Biotechnol* **35**:659–666. doi:10.1038/nbt.3906

380 Mansour AA, Gonçalves JT, Bloyd CW, Li H, Fernandes S, Quang D, Johnston S, Parylak SL, Jin
381 X, Gage FH. 2018. An in vivo model of functional and vascularized human brain
382 organoids. *Nat Biotechnol* **36**:432–441. doi:10.1038/nbt.4127

383 Marton RM, Pașca SP. 2020. Organoid and Assembloid Technologies for Investigating
384 Cellular Crosstalk in Human Brain Development and Disease. *Trends Cell Biol*.
385 doi:10.1016/j.tcb.2019.11.004
386 Matsui TK, Tsuru Y, Hasegawa K, Kuwako K ichiro. 2021. Vascularization of human brain
387 organoids. *Stem Cells* **39**:1017–1024. doi:10.1002/stem.3368
388 Medda X, Mertens L, Versweyveld S, Diels A, Barnham L, Bretteville A, Buist A, Verheyen A,
389 Royaux I, Ebneth A, Cabrera-Socorro A. 2016. Development of a Scalable, High-
390 Throughput-Compatible Assay to Detect Tau Aggregates Using iPSC-Derived Cortical
391 Neurons Maintained in a Three-Dimensional Culture Format. *J Biomol Screen*.
392 doi:10.1177/1087057116638029
393 Molyneaux BJ, Arlotta P, Menezes JRL, Macklis JD. 2007. Neuronal subtype specification in
394 the cerebral cortex. *Nat Rev Neurosci* **8**:427–37. doi:10.1038/nrn2151
395 Nowakowski TJ, Bhaduri A, Pollen AA, Alvarado B, Mostajo-Radji MA, Di Lullo E, Haeussler
396 M, Sandoval-Espinosa C, Liu SJ, Velmeshev D, Ounadjela JR, Shuga J, Wang X, Lim DA,
397 West JA, Leyrat AA, Kent WJ, Kriegstein AR. 2017. Spatiotemporal gene expression
398 trajectories reveal developmental hierarchies of the human cortex. *Science (80-)* **358**.
399 doi:10.1126/science.aap8809
400 Nowakowski TJ, Pollen AA, Sandoval-Espinosa C, Kriegstein AR. 2016. Transformation of the
401 Radial Glia Scaffold Demarcates Two Stages of Human Cerebral Cortex Development.
402 *Neuron* **91**. doi:10.1016/j.neuron.2016.09.005
403 Pagliaro A, Finger R, Zoutendijk I, Bunschuh S, Clevers H, Hendriks D, Artegiani B. 2023.
404 Temporal morphogen gradient-driven neural induction shapes single expanded
405 neuroepithelium brain organoids with enhanced cortical identity. *Nat Commun* **14**.
406 doi:10.1038/s41467-023-43141-1

407 Paşca AM, Sloan SA, Clarke LE, Tian Y, Makinson CD, Huber N, Kim CH, Park J-Y, O'Rourke
408 NA, Nguyen KD, Smith SJ, Huguenard JR, Geschwind DH, Barres BA, Paşca SP. 2015.
409 Functional cortical neurons and astrocytes from human pluripotent stem cells in 3D
410 culture. *Nat Methods*. doi:10.1038/nmeth.3415
411 Paşca SP, Arlotta P, Bateup HS, Camp JG, Cappello S, Gage FH, Knoblich JA, Kriegstein AR,
412 Lancaster MA, Ming G-L, Muotri AR, Park I-H, Reiner O, Song H, Studer L, Temple S,
413 Testa G, Treutlein B, Vaccarino FM. 2022. A nomenclature consensus for nervous
414 system organoids and assembloids. *Nat 2022 6097929* **609**:907–910.
415 doi:10.1038/s41586-022-05219-6
416 Pellegrini L, Bonfio C, Chadwick J, Begum F, Skehel M, Lancaster MA. 2020. Human CNS
417 barrier-forming organoids with cerebrospinal fluid production. *Science (80-)* **369**.
418 doi:10.1126/science.aaz5626
419 Qian X, Nguyen HN, Song MM, Hadiono C, Ogden SC, Hammack C, Yao B, Hamersky GR,
420 Jacob F, Zhong C, Yoon KJ, Jeang W, Lin L, Li Y, Thakor J, Berg DA, Zhang C, Kang E,
421 Chickering M, Nauen D, Ho CY, Wen Z, Christian KM, Shi PY, Maher BJ, Wu H, Jin P,
422 Tang H, Song H, Ming GL. 2016b. Brain-Region-Specific Organoids Using Mini-
423 bioreactors for Modeling ZIKV Exposure. *Cell* **165**:1238–1254.
424 doi:10.1016/j.cell.2016.04.032
425 Qian X, Su Y, Adam CD, Deutschmann AU, Pather SR, Goldberg EM, Su K, Li S, Lu L, Jacob F,
426 Nguyen PTT, Huh S, Hoke A, Swinford-Jackson SE, Wen Z, Gu X, Pierce RC, Wu H, Briand
427 LA, Chen HI, Wolf JA, Song H, Ming G. 2020. Sliced Human Cortical Organoids for
428 Modeling Distinct Cortical Layer Formation. *Cell Stem Cell* **26**:766-781.e9.
429 doi:10.1016/j.stem.2020.02.002
430 Qian Xuyu, Nguyen Ha Nam, Song MM, Hadiono C, Ogden Sarah C., Hammack Christy, Yao

Bing, Hamersky GR, Jacob F, Zhong C, Yoon K, Jeang W, Lin L, Li Yujing, Thakor J, Berg DA, Zhang Ce, Kang E, Chickering M, Nauen David, Ho C-Y, Wen Zhexing, Christian KM, Shi P-Y, Maher Brady J., Wu H, Jin P, Tang Hengli, Song H, Ming G, Bayer A, Lennemann NJ, Ouyang Y, Bramley JC, Morosky S, Marques ETJ, Cherry S, Sadovsky Y, Coyne CB, Ben-Ari Y, Spitzer NC, Blackshaw S, Scholpp S, Placzek M, Ingraham H, Simerly R, Shimogori T, Calvet G, Aguiar RS, Melo AS, Sampaio SA, Filippis I de, Fabri A, Araujo ES, Sequeira PC de, Mendonça MC de, Oliveira L de, al. et, Cauchemez S, Besnard M, Bompard P, Dub T, Guillemette-Artur P, Eyrolle-Guignot D, Salje H, Kerkhove MD Van, Abadie V, Garel C, al. et, Chung S, Hedlund E, Hwang M, Kim DW, Shin BS, Hwang DY, Kang UJ, Isacson O, Kim KS, Danjo T, Eiraku M, Muguruma K, Watanabe K, Kawada M, Yanagawa Y, Rubenstein JL, Sasai Y, Driggers RW, Ho CY, Korhonen EM, Kuivanen S, Jääskeläinen AJ, Smura T, Rosenberg A, Hill DA, DeBiasi RL, Vezina G, al. et, Faria NR, Azevedo RD, Kraemer MU, Souza R, Cunha MS, Hill SC, Thézé J, Bonsall MB, Bowden TA, Rissanen I, al. et, Garcez PP, Loiola EC, Costa RM da, Higa LM, Trindade P, Delvecchio R, Nascimento JM, Brindeiro R, Tanuri A, Rehen SK, Goodwin TJ, Schroeder WF, Wolf DA, Moyer MP, Haddow AD, Schuh AJ, Yasuda CY, Kasper MR, Heang V, Huy R, Guzman H, Tesh RB, Weaver SC, Hansen DV, Lui JH, Parker PR, Kriegstein AR, Heymann DL, Hodgson A, Sall AA, Freedman DO, Staples JE, Althabe F, Baruah K, Mahmud G, Kandun N, Vasconcelos PF, al. et, Jaffe AE, Shin J, Collado-Torres L, Leek JT, Tao R, Li C, Gao Y, Jia Y, Maher B.J., Hyde TM, al. et, Jessup JM, Goodwin TJ, Spaulding G, Kadoshima T, Sakaguchi H, Nakano T, Soen M, Ando S, Eiraku M, Sasai Y, Kim JY, Liu CY, Zhang F, Duan X, Wen Z., Song J, Feighery E, Lu B, Rujescu D, Clair DS, al. et, Kriks S, Shim JW, Piao J, Ganat YM, Wakeman DR, Xie Z, Carrillo-Reid L, Auyeung G, Antonacci C, Buch A, al. et, Kundakovic M, Gudsnuk K, Franks B, Madrid J, Miller RL, Perera FP,

455 Champagne FA, Lancaster MA, Knoblich JA, Lancaster MA, Renner M, Martin CA,
456 Wenzel D, Bicknell LS, Hurles ME, Homfray T, Penninger JM, Jackson AP, Knoblich JA,
457 Lazear HM, Govero J, Smith AM, Platt DJ, Fernandez E, Miner JJ, Diamond MS, Lui JH,
458 Hansen DV, Kriegstein AR, Mariani J, Coppola G, Zhang P, Abyzov A, Provini L, Tomasini
459 L, Amenduni M, Szekely A, Palejev D, Wilson M, al. et, Mlakar J, Korva M, Tul N,
460 Popović M, Poljšak-Prijatelj M, Mraz J, Kolenc M, Rus KR, Vipotnik TV, Vodušek VF, al.
461 et, Muguruma K, Nishiyama A, Kawakami H, Hashimoto K, Sasai Y, Paşca AM, Sloan SA,
462 Clarke LE, Tian Y, Makinson CD, Huber N, Kim CH, Park JY, O'Rourke NA, Nguyen KD, al.
463 et, Petanjek Z, Berger B, Esclapez M, Pollen AA, Nowakowski TJ, Chen J, Retallack H,
464 Sandoval-Espinosa C, Nicholas CR, Shuga J, Liu SJ, Oldham MC, Diaz A, al. et, Roost MS,
465 Iperen L van, Ariyurek Y, Buermans HP, Arindrarto W, Devalla HD, Passier R, Mummery
466 CL, Carlotti F, Koning EJ de, al. et, Tang H., Hammack C., Ogden S.C., Wen Z., Qian X., Li
467 Y., Yao B., Shin J, Zhang F, Lee EM, al. et, Thomsen ER, Mich JK, Yao Z, Hodge RD, Doyle
468 AM, Jang S, Shehata SI, Nelson AM, Shapovalova NV, Levi BP, al. et, Wang W, Lufkin T,
469 Wen Z., Nguyen H.N., Guo Z, Lalli MA, Wang X, Su Y, Kim NS, Yoon KJ, Shin J, Zhang C.,
470 al. et, Yin X, Mead BE, Safaee H, Langer R, Karp JM, Levy O, Yoon KJ, Nguyen H.N.,
471 Ursini G, Zhang F, Kim NS, Wen Z., Makri G, Nauen D., Shin JH, Park Y, al. et, Yu X,
472 Zecevic N. 2016a. Brain-Region-Specific Organoids Using Mini-bioreactors for Modeling
473 ZIKV Exposure. *Cell* **165**:1238–1254. doi:10.1016/j.cell.2016.04.032
474 Quadrato G, Nguyen T, Macosko EZ, Sherwood JL, Min Yang S, Berger DR, Maria N, Scholvin
475 J, Goldman M, Kinney JP, Boyden ES, Lichtman JW, Williams ZM, McCarroll SA, Arlotta
476 P. 2017. Cell diversity and network dynamics in photosensitive human brain organoids.
477 *Nature* **545**:48–53. doi:10.1038/nature22047
478 Renner M, Lancaster MA, Bian S, Choi H, Ku T, Peer A, Chung K, Knoblich JA. 2017. Self-

479 organized developmental patterning and differentiation in cerebral organoids. *EMBO J*
480 **36**:1316–1329. doi:10.15252/embj.201694700
481 Sarkar A, Mei A, Paquola ACM, Stern S, Bardy C, Klug JR, Kim S, Neshat N, Kim HJ, Ku M,
482 Shokhirev MN, Adamowicz DH, Marchetto MC, Jappelli R, Erwin JA, Padmanabhan K,
483 Shtrahman M, Jin X, Gage FH. 2018. Efficient Generation of CA3 Neurons from Human
484 Pluripotent Stem Cells Enables Modeling of Hippocampal Connectivity In Vitro. *Cell*
485 *Stem Cell* **22**:684-697.e9. doi:10.1016/j.stem.2018.04.009
486 Sawada T, Chater TE, Sasagawa Y, Yoshimura M, Fujimori-Tonou N, Tanaka K, Benjamin KJM,
487 Paquola ACM, Erwin JA, Goda Y, Nikaido I, Kato T. 2020. Developmental excitation-
488 inhibition imbalance underlying psychoses revealed by single-cell analyses of
489 discordant twins-derived cerebral organoids. *Mol Psychiatry* **25**:2695–2711.
490 doi:10.1038/s41380-020-0844-z
491 Shi Y, Kirwan P, Smith J, Robinson HPC, Livesey FJ. 2012. Human cerebral cortex
492 development from pluripotent stem cells to functional excitatory synapses. *Nat*
493 *Neurosci* **15**:477–86, S1. doi:10.1038/nn.3041
494 Tidball AM, Niu W, Ma Q, Takla TN, Walker JC, Margolis JL, Mojica-Perez SP, Sudyk R, Deng
495 L, Moore SJ, Chopra R, Shakkottai VG, Murphy GG, Yuan Y, Isom LL, Li JZ, Parent JM.
496 2023. Deriving early single-rosette brain organoids from human pluripotent stem cells.
497 *Stem Cell Reports* **18**:2498–2514. doi:10.1016/j.stemcr.2023.10.020
498 Uzquiano A, Kedaigle AJ, Pigoni M, Paulsen B, Adiconis X, Kim K, Faits T, Nagaraja S, Antón-
499 Bolaños N, Gerhardinger C, Tucewicz A, Murray E, Jin X, Buenrostro J, Chen F, Velasco
500 S, Regev A, Levin JZ, Arlotta P. 2022. Proper acquisition of cell class identity in
501 organoids allows definition of fate specification programs of the human cerebral
502 cortex. *Cell* **185**:3770-3788.e27. doi:10.1016/j.cell.2022.09.010

503 van Esbroeck ACM, Janssen APA, Cognetta AB, Ogasawara D, Shpak G, van der Kroeg M,
504 Kantae V, Baggelaar MP, de Vrij FMS, Deng H, Allarà M, Fezza F, Lin Z, van der Wel T,
505 Soethoudt M, Mock ED, den Dulk H, Baak IL, Florea BI, Hendriks G, De Petrocellis L,
506 Overkleeft HS, Hankemeier T, De Zeeuw CI, Di Marzo V, Maccarrone M, Cravatt BF,
507 Kushner SA, van der Stelt M. 2017. Activity-based protein profiling reveals off-target
508 proteins of the FAAH inhibitor BIA 10-2474. *Science (80-)* **356**:1084–1087.
509 doi:10.1126/science.aaf7497
510 Velasco S, Kedaigle AJ, Simmons SK, Nash A, Rocha M, Quadrato G, Paulsen B, Nguyen L,
511 Adiconis X, Regev A, Levin JZ, Arlotta P. 2019. Individual brain organoids reproducibly
512 form cell diversity of the human cerebral cortex. *Nature* 1. doi:10.1038/s41586-019-
513 1289-x
514 Wang M, Gage FH, Schafer ST. 2023. Transplantation Strategies to Enhance Maturity and
515 Cellular Complexity in Brain Organoids. *Biol Psychiatry* **93**:616–621.
516 doi:10.1016/j.biopsych.2023.01.004
517 Xiang Y, Tanaka Y, Cakir B, Patterson B, Kim K-Y, Sun P, Kang Y-J, Zhong M, Liu X, Patra P, Lee
518 S-H, Weissman SM, Park I-H. 2019. hESC-Derived Thalamic Organoids Form Reciprocal
519 Projections When Fused with Cortical Organoids. *Cell Stem Cell* **24**:487-497.e7.
520 doi:10.1016/J.STEM.2018.12.015
521 Yoon S-J, Elahi LS, Pașca AM, Marton RM, Gordon A, Revah O, Miura Y, Walczak EM,
522 Holdgate GM, Fan HC, Huguenard JR, Geschwind DH, Pașca SP. 2019. Reliability of
523 human cortical organoid generation. *Nat Methods* **16**:75–78. doi:10.1038/s41592-018-
524 0255-0
525 Yuan SH, Martin J, Elia J, Flippin J, Paramban RI, Hefferan MP, Vidal JG, Mu Y, Killian RL,
526 Israel MA, Emre N, Marsala S, Marsala M, Gage FH, Goldstein LSB, Carson CT. 2011.

527 Cell-Surface Marker Signatures for the Isolation of Neural Stem Cells, Glia and Neurons
528 Derived from Human Pluripotent Stem Cells. *PLoS One* **6**:e17540.
529 doi:10.1371/journal.pone.0017540
530 Zhang Y, Pak C, Han Y, Ahlenius H, Zhang Z, Chanda S, Marro S, Patzke C, Acuna C, Covy J, Xu
531 W, Yang N, Danko T, Chen L, Wernig M, Südhof TCCC. 2013. Rapid Single-Step Induction
532 of Functional Neurons from Human Pluripotent Stem Cells. *Neuron* **78**:785–798.
533 doi:10.1016/j.neuron.2013.05.029
534 Zhang Z, Wang X, Park S, Song H, Ming GL. 2023. Development and Application of Brain
535 Region–Specific Organoids for Investigating Psychiatric Disorders. *Biol Psychiatry*
536 **93**:594–605. doi:10.1016/j.biopsych.2022.12.015
537
538
539
540
541
542
543

544 **Figure Titles and Legends**

545 **Figure 1 Adherent cortical organoid model. A** Schematic representation of the
546 differentiation protocol. **B/C/D** Representative NPCs from three different iPSC lines with
547 markers SOX2, Nestin and FOXG1 (scale bar B, 50 µm; C/D, 20 µm). **E** Representative time
548 course showing self-organization during differentiation, starting with radial organization
549 between day 28 and day 42, seeding density 1500 NPCs per well (green is Live-stain from
550 Viability/Cytotoxicity kit; scale bars left to right 100 µm, 150 µm, 100 µm, 100 µm). **F** Full
551 well showing radial organization at day 42 in culture were only a few dead cells are visible in
552 red in the dense centre of the structure, seeding density 1500 NPCs per well (scale bar, 500
553 µm).

554

555

556 **Figure 2 Adherent cortical organoids show an organized network of neuronal and**
557 **astrocyte subtypes. A** MAP2+ somas and dendrites alongside Tau+/MAP2- axons show
558 segregation of dendritic and axonal compartments, with SOX2+ progenitors concentrated in
559 the center of the organoid (Day 75, 200µm). **B** MAP2+ and NeuN+ cells indicate mature
560 neurons (Day 72, 50 µm). **C** Deep-layer cortical marker CTIP2 and upper layer marker CUX1
561 show rudimentary segregation of cortical layers in expected inside-out pattern (Day 64, 50
562 µm). **D** A subset of the MAP2-positive neurons are GAD67+ (white arrows), indicating the
563 presence of an interneuron population in the cortical organoids (Day 60, 50 µm). **E** Astrocyte
564 markers GFAP and S100β show the general radial pattern of astrocyte outgrowth (Day 66,
565 500 µm). **F/G/H** GFAP staining reveals the morphologies of different astrocyte subtypes
566 (white arrows), including fibrous astrocytes (**F**, Day 65, 100 µm), protoplasmic astrocytes (**G**,

567 Day 65, 50 µm) and interlaminar astrocytes (**H**, Day 65, 100 µm). **I** Co-localization of
568 astrocyte marker GFAP and PAX6 marks radial glia (white arrows) (Day 65, 50 µm).
569
570
571 **Figure 3 Adherent cortical organoids form oligodendrocyte lineage cells. A** Adherent
572 cortical organoids show OPCs as early as 44 days, indicated by OPC marker NG2 (Day 44, 20
573 µm). **B/C** The NG2+ OPCs are still present in the cortical organoids after 4 months (Day 119,
574 B 50 µm, C 20 µm). **D** Young oligodendrocytes start to emerge after 4 months indicated by
575 rudimentary MBP staining (Day 119 100 µm and 20 µm). **E/F** After 5 months, MBP-positive
576 oligodendrocytes show more mature morphology and initial wrapping of NF200+ axons (Day
577 148; E, 50 µm and 20 µm, F 5 µm). **G/H/I** Oligodendrocyte distribution at day 161 where the
578 MBP+ oligodendrocytes sit between axons bundles and co-localize with NF200+ axons.
579 (G/H/I Day 161, G 500 µm, H 100µm, I 10 µm)
580
581 **Figure 4 Adherent cortical organoids show synaptic connectivity and network bursts. A**
582 Synapsin staining shows synapse formation along MAP2+ dendrites (Day 70, 20 µm). **B** Co-
583 localization of pre-synaptic marker Synapsin and post-synaptic marker PSD-95 (Day 205, 20
584 µm). **C** MAP2+ dendrites and soma are decorated with Synapsin+ synapses (Day 251, 100
585 µm) **D** Overview of entire well, showing alignment of Synapsin staining with MAP2 (Day 251,
586 500 µm)**.** **E** Sparse labeling of neurons with AAV9.CamKII.eGFP allows detailed imaging of
587 glutamatergic dendritic spines with mature mushroom morphology, contacting pre-synaptic
588 Synapsin puncta (Day 310, 5 µm). **F** Snapshot of radially organized neurons transduced with
589 AAV1.Syn.GCaMP6s.WPRE.SV40 (Day 60, 100 µm). **G** Calcium events per minute from 36
590 cells from 7 recordings (each showing a cluster of neurons) from 2 different cortical

591 organoids at day 61. **H** Network bursts per minute from 37 cells from 6 recordings from 2
592 different cortical organoids. **I** Percentage of events that are part of network bursts indicates
593 that the majority of cells are involved in network burst activity. **J** Representative calcium
594 traces from 2 different clusters in which cells are showing individual activity as well as
595 network bursts where multiple cells are active simultaneously.
596
597 **Supplementary Figure 1 Reproducibility of Neural Progenitor Cells and Adherent Cortical**
598 **Organoids. A** NPCs are positive for SOX2, Nestin, FOXG1, PAX6 and TBR2 (scale bars 20 μm)
599 **B** LIVE/DEAD staining of adherent organoids (N=4) showing reproducibility of the structure
600 formation. Seeding density line 1; 1250 NPCs, line 2; 750 NPCs, line 3; 1000 NPCs (scale bars
601 500 μm). **C** Function of the necessary NPC seeding density to form adherent cortical
602 organoids in relation to the doubling time as a measure of the proliferation rate of the NPCs.
603 The doubling time of the NPCs explains more than half the variation (r^2 = 0.67) of the
604 required seeding density showing that fewer cells need to be seeded for NPC lines with a
605 higher proliferation rate. **D** Proportion of successful, single structure adherent cortical
606 organoids. Each dot represents a different batch of adherent cortical organoids where the
607 size of the batch ranges from 10-40 organoids.
608
609
610 **Supplementary Figure 2 Neuronal maturation in cortical organoids is shown by a temporal**
611 **shift in NPC and neuronal markers. A** Representative images exhibiting change in
612 expression of NPC and neuronal markers over time. Number of cells positive for NPC
613 markers SOX2 and PAX6 decreases over time. Deep-layer CTIP2+ neurons start appearing at
614 day 28, while upper-layer CUX1+ positive neurons appear in higher numbers around day 56.

615 (Scale bars 20 μm). **B** The percentages of DAPI+ cells expressing each of the markers were
616 quantified at four time points. Significant differences between week 2 and week 8
617 expression were seen for SOX2+ (down by 39.6 %), CTIP2+ (up by 13.5 %) and CUX1+ cells
618 (up by 23.1 %). *** $p < 0.0001$, ANOVA one-way followed by Tukey- Kramer's multiple
619 correction test. Error bars indicate SEM, n=3-6 images taken over two wells, for each time
620 point.
621
622 **Supplementary Figure S3 Distribution of axons and dendrites in adherent cortical**
623 **organoids** Radially organized MAP2+/Tau+ dendrites along with both radially and
624 circumferentially organized NF200+/Tau+ axons in duplicate for each cell line (Day 63, scale
625 bars 500 μm)
626
627 **Supplementary Figure S4 Cortical layering in the adherent cortical organoids A**
628 Rudimentary separation of SOX2+ NPCs, CTIP2+ deep layer neurons and CUX1+ upper layer
629 neurons (Day 67, scale bar 100 μm) **B-E** Separation of CUX1 and CUX2 expression (B day 70,
630 scale bar 100 μm; C day 70, scale bar 500 μm; D day 67, scale bar 500 μm; E day 67, scale
631 bar 100 μm)
632
633 **Supplementary Figure S5 GAD67+ interneurons make up a small proportion of NeuN+**
634 **neurons in the adherent cortical organoids A** Example image of GAD67+ interneuron
635 proportion of NeuN+ neurons (Day 67, 50 μm). **B** Quantification of GAD67+ proportion of
636 NeuN+ neurons. Every point is the percentage of GAD67+ interneurons out of all NeuN+
637 neurons in a spatially randomized selected image with on average 130.6 (± 16.1) NeuN+

638 nuclei per frame. (Line 1: N= 26 images of 6 different cortical organoids at day 65-67; Line
639 2/3: 6 images of 2 different organoids at day 65).
640
641 **Supplementary Figure S6 Astrocyte distribution within Adherent Cortical Organoids** The
642 abundantly present GFAP+ and S100B+ astrocytes have a comparable distribution with the
643 MAP2+ neurons in the adherent cortical organoids. The astrocytes show radial patterns with
644 many somas located in the centre as well as a large presence outside the centre (Day 63,
645 scale bars 500 µm).
646
647 **Figure 4 – Video 1**
648 Video showing 10 minutes of calcium imaging of an adherent cortical organoid at Day 61
649 using the genetically encoded calcium indicator AAV1.Syn.GCaMP6s.WPRE.SV40 (rainbow
650 filter indicates increasing calcium signal ranging from blue to red, speed increase indicated
651 by time stamp in top left corner).
652
653

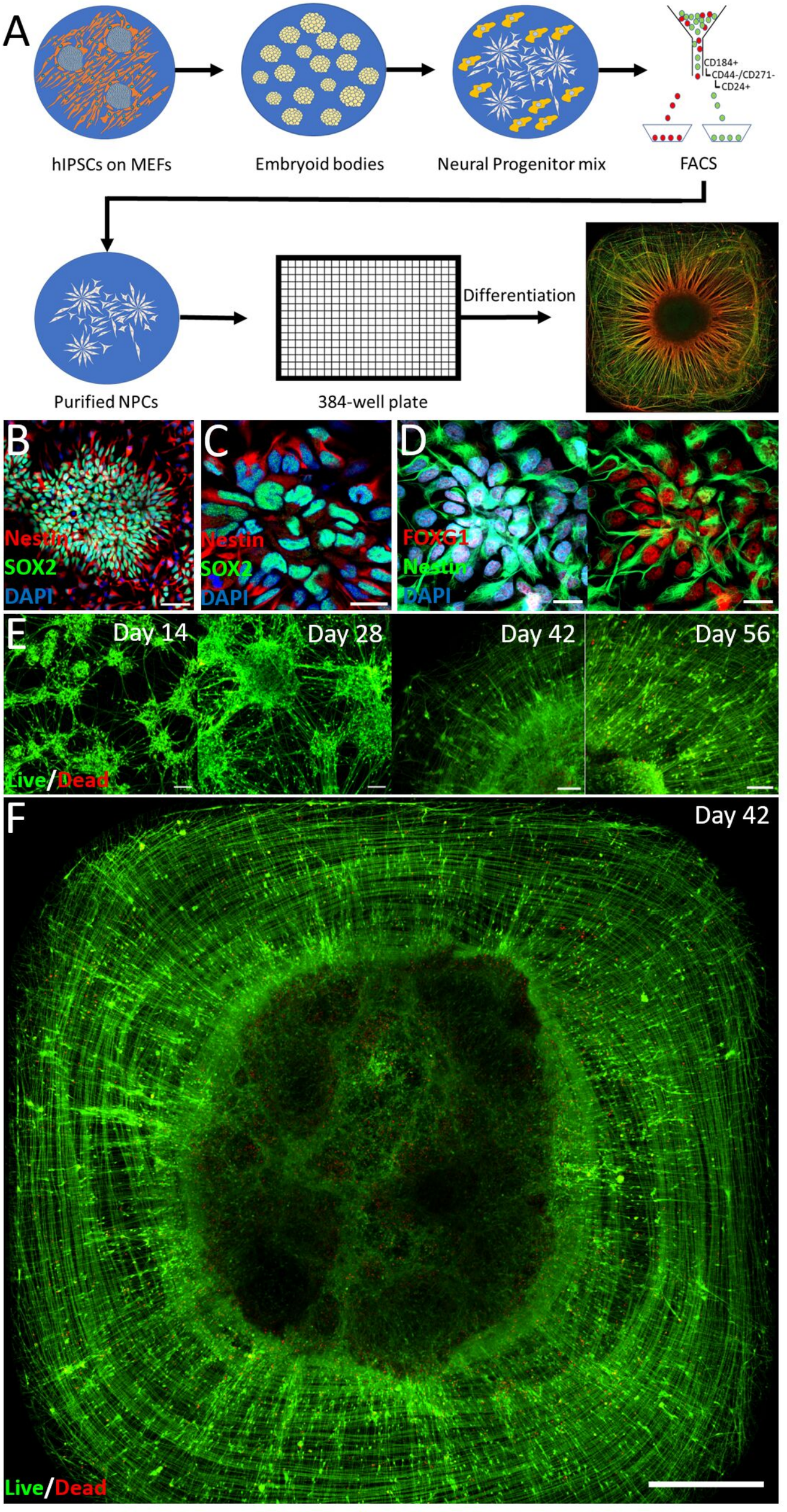
A
hIPSCs on MEFs
Embryoid bodies
Neural Progenitor mix
CD184+
CD44-/CD271-
CD24+
FACS
Purified NPCs
384-well plate
Differentiation
B
Nestin
SOX2
DAPI
C
Nestin
SOX2
DAPI
D
FOXG1
Nestin
DAPI
E
Day 14
Day 28
Day 42
Day 56
Live/Dead
F
Day 42
Live/Dead

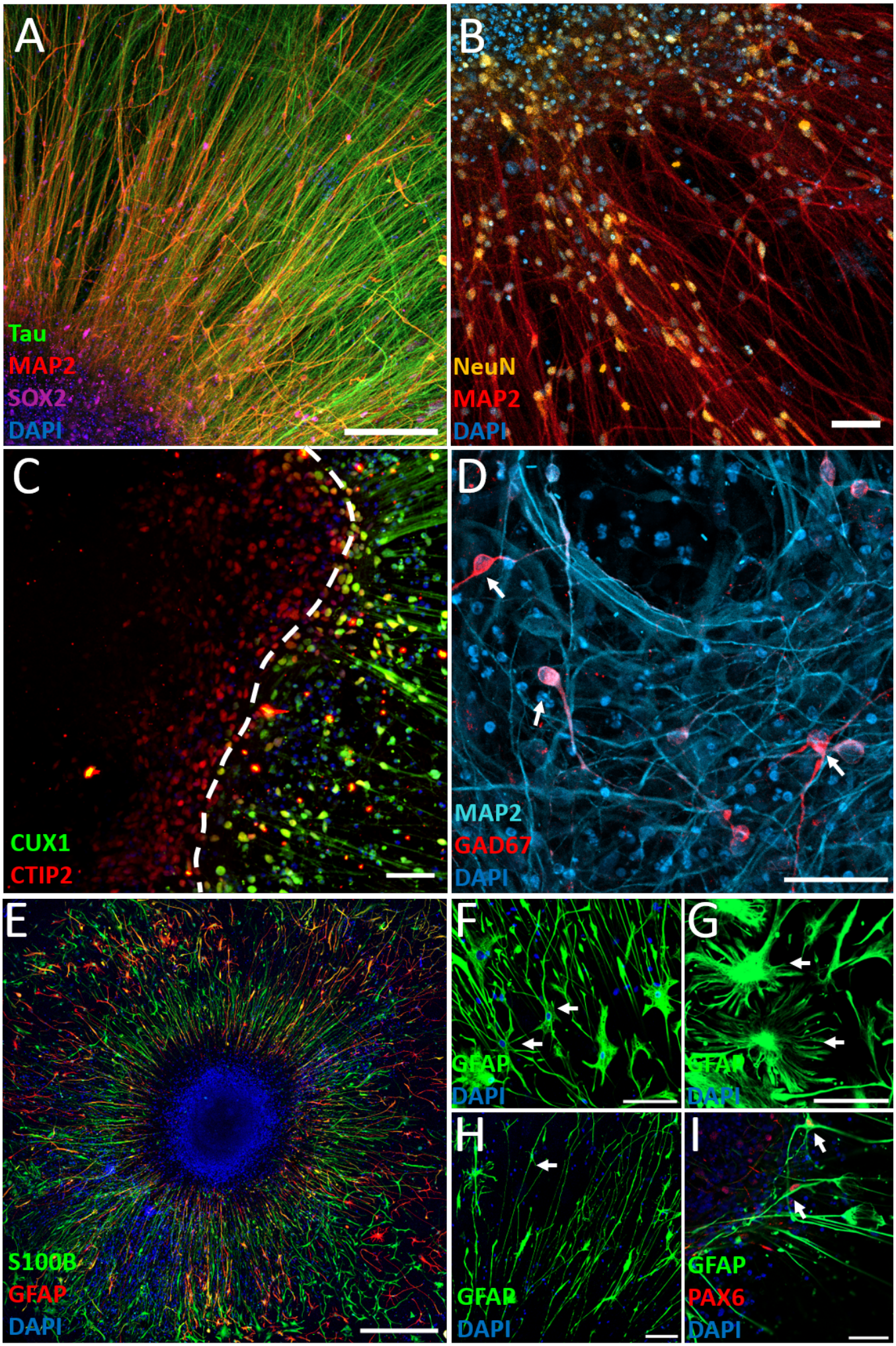
A
Tau
MAP2
SOX2
DAPI
B
NeuN
MAP2
DAPI
C
CUX1
CTIP2
D
MAP2
GAD67
DAPI
E
S100B
GFAP
DAPI
F
GFAP
DAPI
G
GFAP
DAPI
H
GFAP
DAPI
I
GFAP
PAX6
DAPI

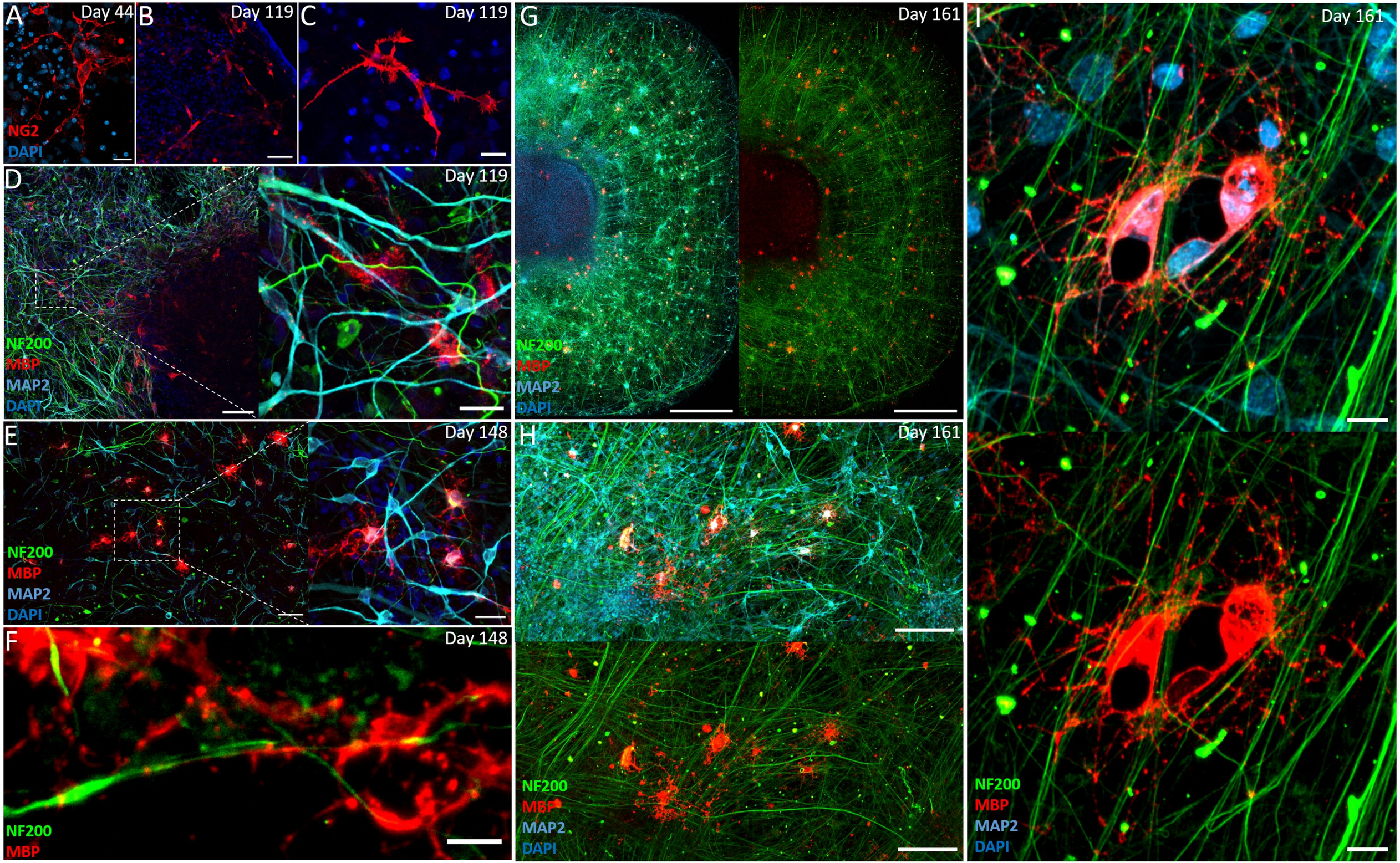
A
Day 44
NG2
DAPI
B
Day 119
C
Day 119
D
Day 119
NF200
MBP
MAP2
DAPI
E
Day 148
NF200
MBP
MAP2
DAPI
F
Day 148
NF200
MBP
G
Day 161
NF200
MBP
MAP2
DAPI
H
Day 161
NF200
MBP
MAP2
DAPI
I
Day 161
NF200
MBP
MAP2
DAPI

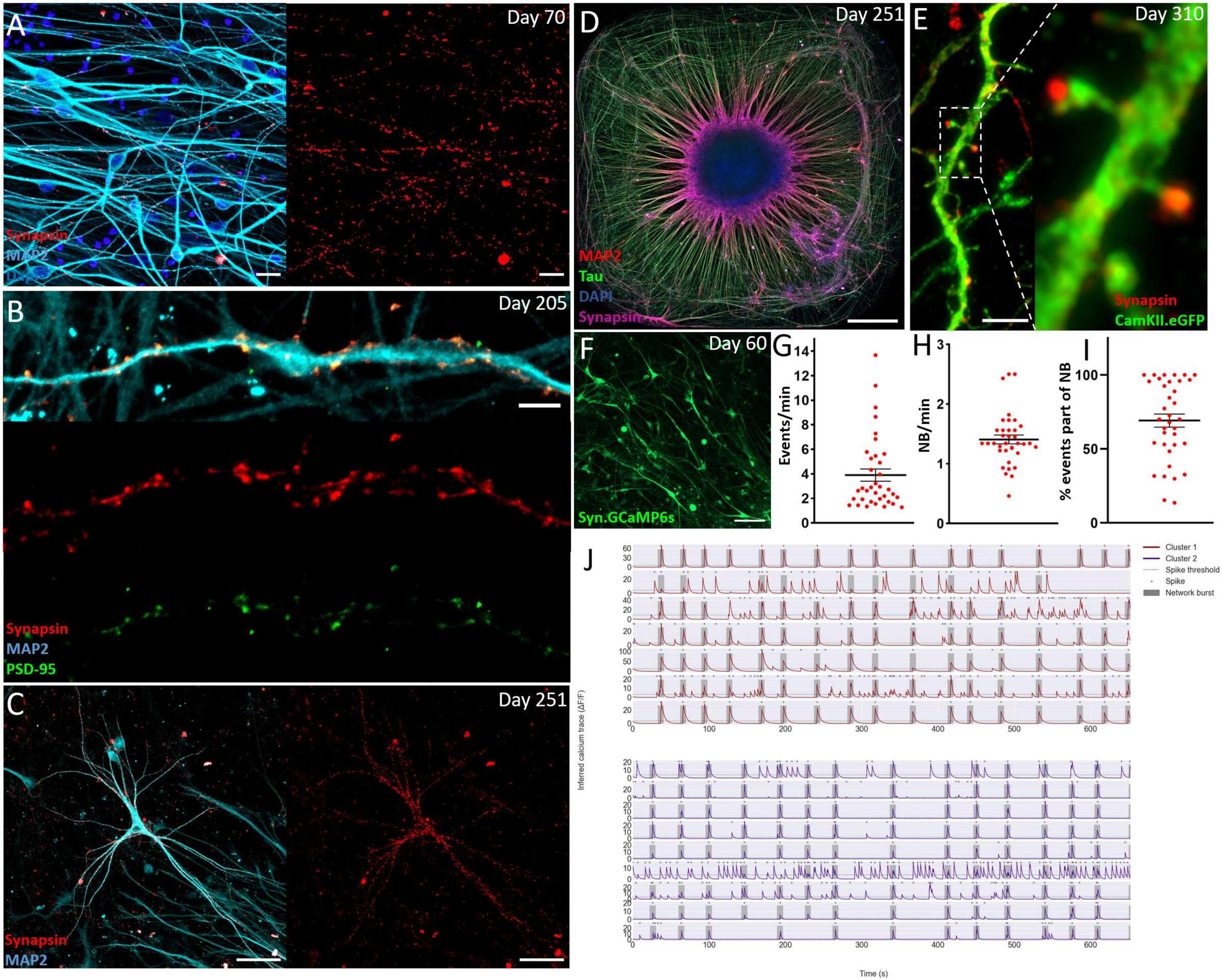
A
Day 70
Synapsin
MAP2
DAPI
B
Day 205
Synapsin
MAP2
PSD-95
C
Day 251
Synapsin
MAP2
D
Day 251
MAP2
Tau
DAPI
Synapsin
E
Day 310
Synapsin
CamKII.eGFP
F
Day 60
Syn.GCaMP6s
G
Events/min
H
NB/min
I
% events part of NB
J
Cluster 1
Cluster 2
Spike threshold
Spike
Network burst
Inferred calcium trace (ΔF/F)
Time (s)